

Article

Identifying storm hotspots and the most unsettled areas in Barcelona by analysing significant rainfall episodes in Barcelona during the 2013 – 2018 period.

Laura Esbrí ^{1,*}, Tomeu Rigo ², María Carmen Llasat ¹, and Blanca Aznar ³

¹ GAMA team, Department of Applied Physics, University of Barcelona, Spain; lesbri@meteo.ub.edu

² Meteorological Service of Catalonia (Servei Meteorològic de Catalunya - SMC), Barcelona, Spain

³ Barcelona Cicle de l'Aigua S.A. (BCASA), Barcelona Spain

* Correspondence: lesbri@meteo.ub.edu

Abstract: Flash floods repeatedly threaten Barcelona, damaging the city infrastructure and endangering the safety of the population. The city's urban planning and socioeconomic distribution, associated with the topography and other geographic factors, means that these flood events do not affect the entire city in the same way. This is a key point for surveillance and emergency tasks, which need some patterns and models to improve response capacity. This work aims to gain a better understanding of such events, to add valuable information on how to predict and manage these situations. For this purpose, both radar and ground observational data have been combined to identify the most important precipitation episodes in Barcelona between 2013 and 2018. To make the analysis easier, a new algorithm has been developed to determine the thunderstorm hotspots. Episodes with a higher impact have been analysed in depth. The final objective is to improve the actions taken by the organisation responsible for managing urban floods, which have seen Barcelona recognised as a model city for flood resilience by the United Nations.

Keywords: flash floods; urban floods; storms; hazard management; urban hydrology; convection; convective cells; thunderstorms; radar; flood prevention; Mediterranean

1. Introduction

Hydrometeorological hazards especially affect the Mediterranean basin, where intense rainfall, which produces flash floods, plays an important role. Most of the floods are concentrated inside a geographical belt that runs from the western Mediterranean to the Black Sea [1]. In Catalonia (NE of the Iberian Peninsula, and NW of the Mediterranean Basin), floods are the most damaging natural hazard [2], with a mean rate of over eight flood episodes per year [3]. During the 1981-2015 period, more than 250 cases were identified, most of them near the coastline [3–5]. As a result, the Spanish Insurance Compensation Consortium (in Spanish, Consorcio de Compensación de Seguros - CCS) paid out over 450 million euros between 1996 and 2015. Furthermore, other private insurance expenses must be added. Highly convective and very localised precipitation is responsible for 70% of the flood episodes along the Catalan coast [6,7], affecting the most densely populated Catalan counties in 1 out of 3 cases.

According to the flood classification in Barrera et al. [8], 36% of Catalan floods were ordinary, 53% could be considered extraordinary [9] and 11% were catastrophic (1981-2010 period). There is no significant trend related to catastrophic floods in Catalonia, but the number of extraordinary floods has increased in recent years [3,8–10]. Explaining this trend requires taking into account not only hydrometeorological hazards but also vulner-

ability, exposure and coping capacity [11–14]. Still, recent studies point towards an increase in flood risk but, more to an increase in the associated socioeconomic impact [15]. To increase flood prevention and resilience, strong social commitment and sustainable efforts are needed [16]. This can only be achieved through better empowerment and co-responsibility at every level, based on an improved knowledge of prevention and prediction [17].

A study on regions in the United States by Naylor and Sexton [18], concludes that the urbanisation of metropolitan areas may have changed the location of convective storm-cells and precipitation fields. In the Mediterranean region, there is a significant interaction between urbanisation and convective precipitation, as most floods are caused by very heavy and local precipitation in urbanised areas [7]. The topographic characteristics of the Mediterranean region, in combination with its geographical location and the presence of a warm sea, mean that dangerous convective systems can develop, or unsettled Atlantic perturbations can be strengthened [19]. Rigo and Llasat [20] determined that Mesoscale Convective Systems (MCS) and multicellular systems are responsible for the most significant floods in Catalonia, while isolated convection or multicellular systems produce local and heavy rainfall and consequently cause flash floods [7]. To be managed as well as possible, good meteorological forecasts and primary warning systems are required. Numerical weather predictions are usually not accurate for such small scales with complicated orography, and advanced monitoring systems have limitations as well. New and more advanced decision support systems are needed to provide valuable information in critical situations [1].

In this context, radar data offers good complementary information, and can work as an observational system and also as an assimilating source for meteorological models [21,22]. Radar networks provide reflectivity compositions with wide spatial coverage and a continuous timeline. This information helps MCS to be better understood in the Mediterranean region [23] by providing information about rainfall fields and rainfall intensity. Even so, rainfall amount is usually underestimated by radar calculations, which increases with range and beam blocking [24]. A rain gauge network with good coverage provides useful information about rainfall properties in the region of interest [3], and can be quite useful to manage rainfall alerts in real time. But there are some downsides when working with rain gauge data: devices are prone to malfunction if they are not under constant review and an additional and high-density network is necessary to reproduce small scale variability in rainfall [25].

The main objective of the present work is to determine whether storm cells are more concentrated in some areas of Barcelona than in others. In the first step, radar data will be combined with observations from rain gauges to find significant rainfall episodes in Barcelona. Secondly, a new radar-based methodology is developed to identify convective cells in those relevant episodes, and a further study is carried out to localise the areas of the city where convective cells are most frequently located. The identification and characterisation of storms aims to increase understanding to improve short-term forecasts. The performance of early warning systems will improve in conjunction with better forecasts, reducing the impact of severe weather.

Section 2 details the different data sources and explains the methodology. Then in Section 3, all the different results are shown and discussed. Finally, Section 4 includes a summary, and final conclusions are reached.

2. Data and Methodology

This section first describes the region of study and explains the water cycle management system in Barcelona. Then it goes on to share the data sources and finally, detail the methodology.

2.1. Region of interest

The Barcelona Metropolitan Area (AMB) belongs to the Mediterranean basin, in the northeast of the Iberian Peninsula, about 120 km to the south of the Pyrenees (Figure 1). It covers more than 600 km² and it is densely urbanised (36 municipalities comprising over 3.2 million people) with very frequent heavy rainfall events. Two mechanisms favour flash floods in this area: heavy precipitation caused by orographic effects, and a topographic relief that encourages flux concentration and convergence [1]. In turn, Barcelona city (Figure 2) is naturally limited by the Mediterranean Sea (east), the Collserola mountain range (west), the river Llobregat (south) and the river Besòs (north). It is the second most populated city in Spain with more than 1,600,000 inhabitants (2018). It covers around 101 km². Floods are relatively frequent in the city, with more than 3 pluvial flood episodes per year (109 flood events were registered between 1981–2015 according to [17]). In general, they cause damage to basements and ground floors, power outages, and create problems for urban traffic and public transportation. Floods can even affect historical or heritage buildings, given their locations in flood prone areas.

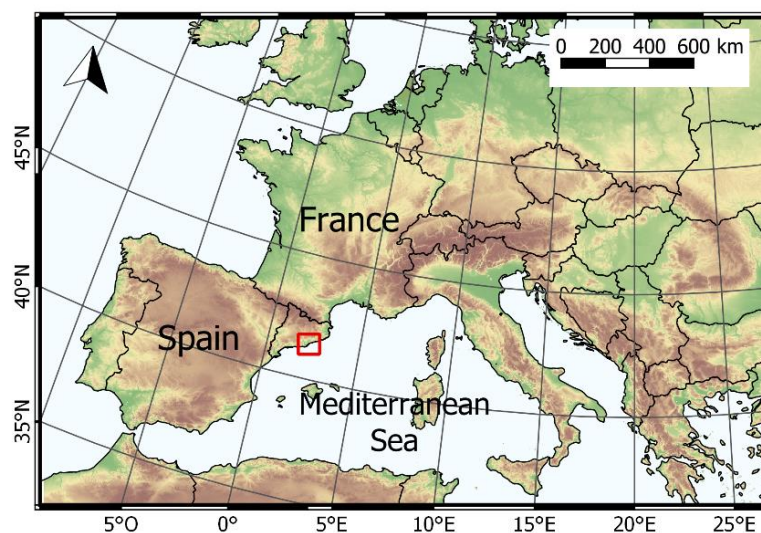


Figure 1: Geographical location of Catalonia and the Region of Interest (ROI) inside Europe and the Mediterranean basin.

In the present study, the comparison between radar data, surface observations and the impact of damage will focus on Barcelona city and Cornellà (see section 2.3.2 for more details). The latter area (the cities of Barcelona and Cornellà) will be referenced as the Region of Interest (ROI). Nevertheless, to have a better understanding of the phenomena within the ROI, the analysed area for each episode from a radar point of view has been extended about 10 km² from the ROI (Figure 2).

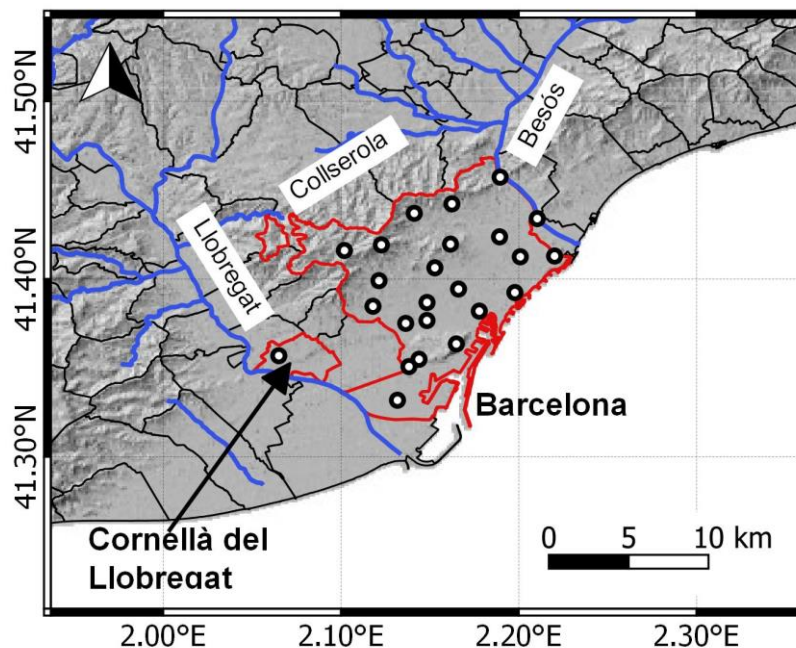


Figure 2: ROI and the surrounding area of around 10 km² that represent the region of study. The white dots are the rain gauge locations of the BCASA network. Also, the main rivers surrounding Barcelona (Llobregat and Besòs) are labelled, as well as the main mountain range (Collserola).

2. 2. Water cycle management and alert system in Barcelona

The first attempt to improve resilience to city floods in Barcelona was in 1988 with the design of a specific sewerage plan (within the context of the 1992 Olympics) that aimed to favour water evacuation off the streets by means of building large water collectors near the sea (breakwaters). On 1992, Barcelona City Council promoted a consortium partnership to complete the task, Clavaguera de Barcelona S.A. (CLABSA, nowadays Barcelona Cicle de l'Aigua S.A., BCASA). Some time later, on 21 September 1995, a flood caused one death and the city collapsed (2,500 emergency calls, 25 flooded metro stations, 80 incidents in the sewer system, etc.) because of a local cumulative rainfall of 91.9 mm and a maximum 5-min rainfall intensity rate of 235 mm/h [26]. That unfortunate flood event showed the need for more actions to improve the management of intense rainfall events in the city. In 1997, BCASA published a new specific sewerage plan for Barcelona (PECLAB'97) diagnosing the drainage problems in the city and proposing a new series of actions for improvement. From 1997 to 2004 a series of slide gates and underground storm water retention tanks were built, and rain gauges began to be installed in several locations in the city. Also, a remote system to control the slide gates and water tanks was implemented. Overall, the system was designed to prevent floods for 10-year event precipitation, and even at some points for a 50-year event [27]. In 2014, Barcelona City Council decided to turn the CLABSA consortium into a public enterprise to manage the entire water cycle in the city: Barcelona Cicle de l'Aigua S.A. (BCASA). They handle all the related water processes: sewerage, rainwater tanks, groundwater system, sea water quality control, flooding risk at riverside parks and rainfall intensity warnings.

Nowadays, BCASA manages 13 underground water tanks and 2 surface flooding areas with a capacity for 477,010 m³. They also monitor real-time rainfall data from their rain gauge network, compounded by 23 Lambrecht and Geónica tipping bucket sensors (with an accuracy of 0.1 mm), that cover the entire area of Barcelona (Figure 2). The prediction team at BCASA is always informed with the latest weather forecast and the radar weather

observations from the Meteorological Service of Catalonia (SMC) along with nearly real-time rain gauge data from the network (5-min. updating frequency). The automatic alert system processes the data from the rain gauge network and, based on 20-minute and 60-minute rainfall intensities (maximum and average), it issues five different alert levels for Barcelona (NAB) (Table 1). The first three levels act as a warning, so the current automatic protocols are revised by experts and the different contributors to emergency prevention and mitigation are revised to ensure the situation is being controlled automatically, with no incidents. Level four suggests that Civil Protection should activate the Alert Plan for possible floods in Barcelona. Finally, level five activates an emergency, and the expert committee meets to coordinate the situation in the city. At this point, BCASA contributes as an information provider and experienced consultant.

Table 1: BCASA criteria to activate the alert level in Barcelona (NAB). Levels are based on two precipitation intensity thresholds (20 min. intensity, I_{20} and 60 min. intensity, I_{60}). PAB = Forecast of a possible alert Barcelona.

	NAB	PAB	Rainfall Level	
			High Intensity indicator (I_{20})	Prolonged rain indicator (I_{60})
0	INACTIVE	0	-	-
1	STANDBY	1,2	0 mm/h ($T_{20} > 0$)	0 mm/h ($T_{60} > 0$)
2	SURVEILLANCE		20 mm/h ($T_{20} < 0,1$)	10 mm/h ($T_{60} < 0,1$)
3	PRE-ALERT	≥ 3	30 mm/h ($T_{20} \approx 0.15$)	15 mm/h ($T_{60} \approx 0.15$)
4	ALERT		50 mm/h ($T_{20} \approx 0.4$)	25 mm/h ($T_{60} \approx 0.4$)
5	EMERGENCY		70 mm/h ($T_{20} \approx 1$)	35 mm/h ($T_{60} \approx 1$)

The average number of alerts activated per year is between 3 and 4, but it varies from one year to the next. Also, as urban floods in Barcelona have very short time scales and are rapidly solved, the emergency level is rarely activated. The combination of the automatic sewerage and drainage systems, along with an alert protocol, allows a coordinated effort with Civil Protection and authorities when flash floods occur in the city.

2.3. Data sources

2.2.1. Radar data from the Meteorological Service of Catalonia(SMC)

Radar data used in this study belong to the radar network of Meteorological Service of Catalonia (XRAD). XRAD is composed of four radars distributed in strategic points throughout Catalonia (Figure 3): Puig Bernat in Vallirana (PBE, installed in 2000), Puig d'Arques in Cruïlles, Monells and Sant Sadurní de l'Heura (PDA, 2002), la Creu del vent in La Panadella, Montmaneu (CDV, 2003) and La Miranda, in Tivissa-Llaberia (LMI, 2008). Each of them works on three tasks: one long-range task (250 km), which operates at a set of elevations that are part of the radar volume with similar characteristics, and two short-range tasks (130-150 km), from which different products are created. Composite products are created from individual radar products. They cover the whole region of Catalonia and its surroundings (Figure 3).

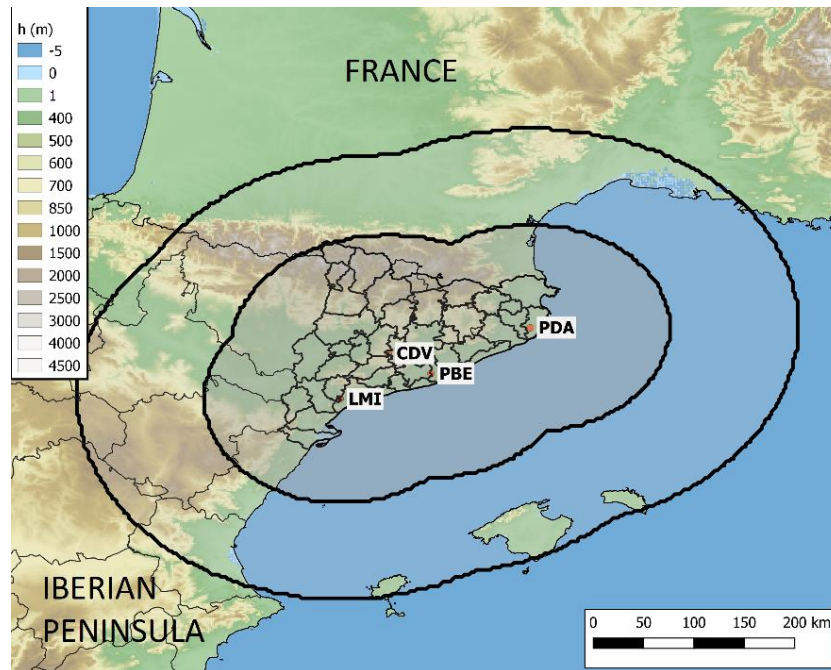


Figure 3: Map showing the north-eastern Iberian Peninsula and southern France. The black outer line represents long-range coverage of XRAD, and the inner line represents the short-range coverage. The labels and orange dots correspond to each XRAD radar. LMI (La Miranda), CDV (Creu del vent), PBE (La Panadell), and PDA (Puig d'Arques i Cruïlles).

All radar products used here are a composition of the four different radars. The first one is the daily Quantitative Precipitation Estimation (QPE), corrected with EHIMI (Hydrometeorological Integrated Forecasting Tool) [23] and observational data from the Automatic Weather Stations network of the SMC (XEMA). It is a short-range product with $1 \times 1 \text{ km}^2$ spatial resolution. Data files have been available in 'GeoTIFF' format since 2013. In a second stage, to identify convective cells, the maximum surface reflectivity compositions, and short-range reflectivity compositions on 10 vertical levels, CAPPIs (Plan Position Indicator of Constant Altitude), are also used. This product has a vertical extension between 1 km and 10 km (by 1 km) and has a time resolution of 6 min and a spatial resolution of $2 \times 2 \text{ km}^2$. Considering all vertical levels available adds more robustness to the method when identifying convective cells than when only considering the lowest levels (see section 2.3.4).

2.2.2. BCASA rain gauge network and database

As mentioned in Section 2.1, the rain gauge data for each rocker device from the BCASA network (Figure 2) is stored in a database. As the network is composed of tipping bucket devices, the information is stored when the bucket fills up and turns over. This information must be converted to minute intensities or hourly rainfall accumulations, depending on how it will be applied. Since 2011, there has also been a separate database with post-event rainfall reports for all the different episodes that have exceeded the rainfall volume of 1 mm (in the same device). This second database includes the date of occurrence, average and maximum precipitation, average and maximum 20-minute and 60-minute intensities, and NAB for the episode proposed by BCASA (Table 1). When the NAB reaches or exceeds level 3, related incidents are requested from Barcelona City Council and are also included on the database. These incidents are usually related to the sewer system, but they also include flooding on streets, in the metro and in basements.

Hourly rainfall data from the rain gauge network was used in the study to calculate 24-hour rainfall accumulation. This data was cleaned and prepared in advance for the purposes of the study. The rainfall reports are also used to classify rainfall events in Barcelona into different categories according to its impact by means of NAB.

2.3. Methodology

Diagram showing the different steps followed in the present study, in Figure 4. In the following subsections, every process is explained in greater detail.

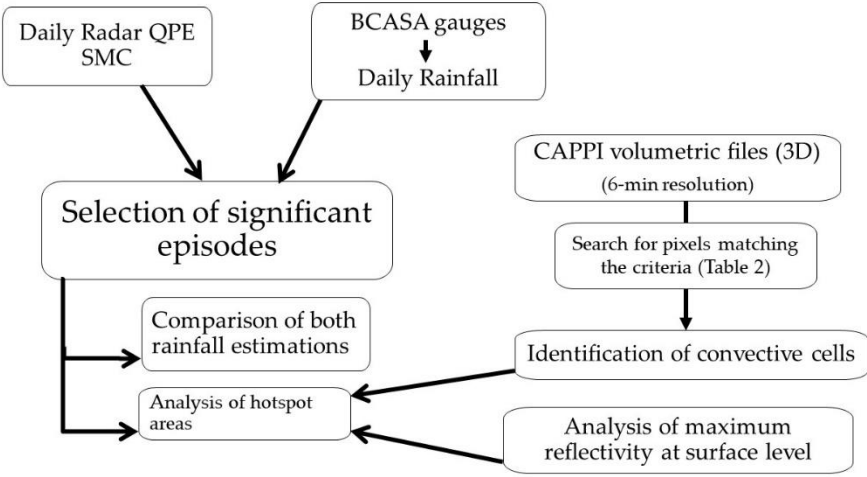


Figure 4: Conceptual scheme of the followed methodology

2.3.1. Database creation: Rainfall episodes inside ROI

The first objective is to identify all the relevant rainfall episodes inside the ROI (cities of Barcelona and Cornellà de Llobregat) to create the database for the period of study. For the purposes of this study, a rainfall episode is defined as a single rainfall day in which at least 10 mm of accumulated rain is exceeded at a given point. The location of this point must be inside the ROI. Rainfall accumulations are calculated between 00:00 UTC and 23:59 UTC for a single day. If the precipitation continues after 23:59 UTC, two different episodes are identified. SMC started to generate volumetric georeferenced radar files (with the actual format) at the beginning of 2013, but during the first few months some adjustments had to be made. It is for this reason that the period of study is from April 2013 to December 2018. Following this criteria, episodes are identified from XRAD data by analysing the maximum accumulated QPE over 24 hours (P_{max}) for each pixel of the radar frame. The identification of episodes is then repeated, selecting the days that meet the criteria from the list of rainfall reports (with rain gauge data) from BCASA. Episodes obtained from both sources are then compared. If episodes do not appear in both lists, an analysis is carried out to determine if the rainfall within the ROI was significant, or if it was an inaccuracy in the data from one of the systems.

To analyse the episodes that caused major stress to the city in more detail, episodes were selected based on BCASA NAB criteria (Table 1). The selected episodes were those for which BCASA issued an NAB alert level greater than or equal to 3. Furthermore, to have a more complete view of the impact on the city, rain reported incidents related to the episodes were requested from BCASA for the studied period (April 2013 to December 2018). The original data from reported incidents belonged to Barcelona City Council.

2.3.2. Comparison of rain gauge data and radar data for rainfall episodes

Rain gauge data is only available for the specific locations where devices are installed. So, when comparing with data from the radar network, radar QPE values must be extracted for each episode on the same coordinates (longitude and latitude) where the BCASA rain gauges are located. Using similar statistics as Trapero et al. [24,28], the Bias (expressed in mm) and the Root Mean Square Factor (RMSf) were calculated for each rainfall episode:

$$BIAS = \frac{1}{N} \sum_{i=1}^n 10 * \log \left[\frac{QPE_{rad}}{QPE_{gau}} \right] \quad (1)$$

$$RMSf = \sqrt{\frac{1}{N} \sum_{i=1}^n \left(\ln \left[\frac{QPE_{rad}}{QPE_{gau}} \right] \right)^2} \quad (2)$$

where N is the number of points where either QPE_{rad} and QPE_{gau} are greater than 0.1 mm. The RMSf is a dispersion indicator, so it should be larger whenever the episode has high variability. That will happen if the rainfall episode is highly convective. Otherwise, if Bias is close to zero, radar and rain gauges agree in rainfall accumulations while Bias values smaller or greater than zero will indicate either that the radar underestimated or overestimated the rainfall amounts.

2.3.4. Analysis of storm hotspots with radar

At this point, two approaches are applied to the previously identified significant episodes in order to test whether there are areas inside the ROI where intense rainfall is most prone to occur.

On the one hand, radar data files containing maximum reflectivity intensities for an episode (24h) at surface level were analysed for significant episodes. For each radar file (containing the maximum values of surface reflectivity for the day), three different thresholds of maximum surface reflectivity were established: 30 dBZ, 45 dBZ and 55 dBZ. Any pixels surpassing the tested threshold during an episode were counted and then added up if the threshold was also surpassed for the same pixels for another episode. The results for each threshold show the number of episodes that surpassed the threshold for each pixel (1x1 km²). Those products will be shown for each threshold, where maximum surface reflectivity values were observed with a higher frequency when a significant episode took place.

The other approach is to establish a very simple radar-based methodology to identify and locate convective storm cells for significant episodes (if any). For this task, CAPPI products from XRAD were used. As explained in Section 2.2.1, these are volumetric files containing different vertical levels of reflectivity at a time resolution of 6 minutes. The algorithm was programmed as an R script and follows the subsequent procedure for each one of the files:

1. It searches for pixels (2x2 km²) inside Barcelona and the surrounding area (a radius about 10 km from the limits of the city), that simultaneously: surpass the threshold of 35 dBZ for the maximum reflectivity value, achieve at least 30 dBZ of reflectivity above 3 km of altitude, and where at least 5 contiguous pixels match the criteria.
2. All the adjacent pixels that meet these conditions will be grouped into a single convective cell. If more than one convective cell is identified in the same data-file, different coexisting convective cells will be considered.
3. The information characterising the convective cell is stored with one entry into a text-file. This information covers: the date of the event, the time when the cell was detected, the longitude and latitude coordinates of the centre of the cell, how many

pixels it is made of, the overall area, and if there were other cells at the same time inside the analysed area.

The restriction of the minimum number of pixels to meet the reflectivity conditions is imposed to avoid isolated maxima of reflectivity without enough organisation to be considered a convective storm cell. Both [29] or [30] proposed more robust methods to identify convective storm cells with 3D algorithms. However, the present work has greater robustness than other 2D algorithms [31,32] as the altitude of convective structures has also been taken into account, following a simplified 3D algorithm. The main reason for applying this methodology is its computational efficiency, which allows analysis of a very large number of episodes.

3. Results and discussion

3.1. Database creation: rainfall episodes

Between April 2013 and December 2018, 163 rainfall episodes that met the criteria (section 2.3.1) were found in both data sets (XRAD and BCASA networks). However, there were 58 additional episodes detected only by radar. For those episodes, a deeper analysis was carried out concluding the following:

- In 38 cases, BCASA rainfall observations registered precipitation between 1 and 10 mm at some point.
- In 6 cases, rainfall collection by the BCASA network was under 1 mm, but radar showed a consistent rainfall field.
- In a further 14 cases, the algorithm used classified the day as a rainfall episode, but the rainfall field barely crossed the border of ROI, or rainfall occurred mainly over the sea. These cases were not included on the final list of episodes.
- Major differences in the number of episodes between both sources were shown by the end of spring and the beginning of autumn: a difference of 9 episodes in June, 12 in July, 11 in September and 12 in October. Summer events are usually very convective, short and local, and for this reason they may not be detected by the rain gauge network. Despite the rain gauge network having a good spatial resolution, convective precipitation can be highly localised and in some cases is not detected with any available surface sensor [33]. The resulting final list is made up of 207 rainfall episodes within the ROI for the studied period (shown on Appendix A, Table A.1).

From now on, the selected episodes will be referred to as rainfall episodes in the ROI. The climatology for these significant episodes is shown on Figure 5. December is the month with the least episodes, and September has the most. Overall, from February to August, there are between 12 and 18 episodes per month. It is during autumn (from September to November) when the greater numbers of episodes are found.

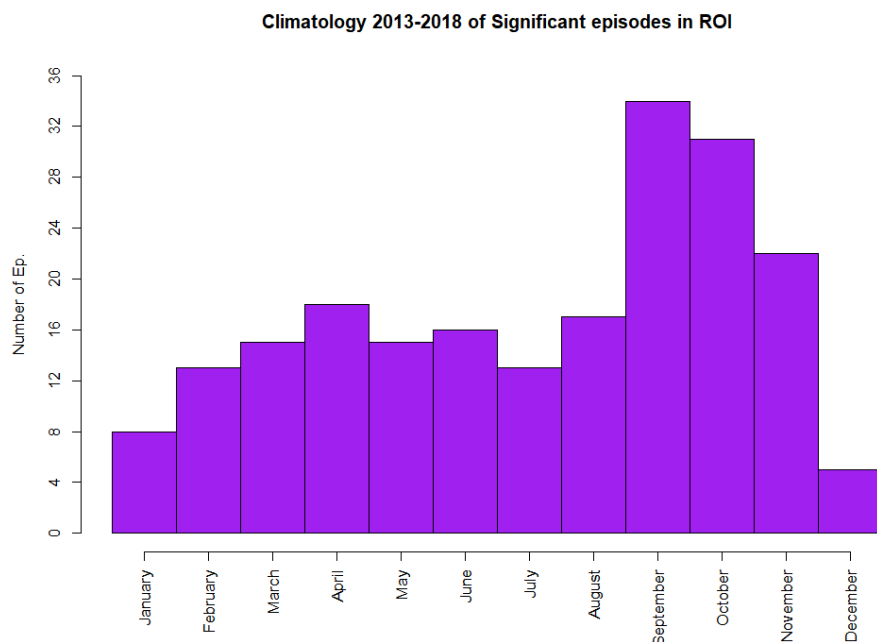


Figure 5: Climatology for the significant episodes from April 2013 to December 2018.

The climatology of significant rainfall episodes in this work is consistent with previous studies carried out in the same region for longer study periods. In Catalonia there is a large spatial and temporal variability in terms of the annual rainfall cycle, with typically short thunderstorms during summer and spring and larger events during late autumn and winter [20,33]. Also, Barrera et al. [8] and Cortès et al. [5] showed that most of the floods in Barcelona are concentrated between the end of summer and autumn, with the maximum number of episodes per month in September.

When filtering rainfall episodes using the NAB level issued by BCASA, that are greater than or equal to 3, there were 64 cases in the studied period (Table A.2 in the appendix A). Analysing the dates for the episodes with the highest alert level (NAB = 4) on Table A.2, one observe they are not uniformly distributed along the year. They seem more likely to occur from July to November, but since there are only 17 cases over a 6-year period it is not possible to determine any kind of trend. Referring those with NAB equal to 3, the probability of occurrence is higher from May to November, with a maximum average of cases per month in August and September. These results are consistent with [33]. According to the data, there is no evidence of an upward trend for episodes with greater NAB, but again, the study period is too short.

NAB is an alert indicator, but it is not directly related to the consequences for the city or to actual hazards. For this reason, incidents reported to Barcelona City Council are also included for those episodes (Table A.2 in the appendix). It stands out that not all the episodes with the highest precipitation values had the most reported incidents. In fact, incidents were only reported for 28 of them. The first four episodes that reported the largest number of events took place in the last year of the study (2018). From October to November of the same year there was an unusually high occurrence of extraordinary rainfall episodes in the city. In general, NAB = 4 cases have more reported incidents per episode than NAB = 3 ones. These episodes were mainly concentrated in November, March, September and October. Considering the total number of incidents per year, 2018 (with 353) was the most reported year. The second was 2014 (174), then 2017 (75), 2016 (58), 2015 (17) and finally 2013 (15). Since 2013, there has been an increasing trend in the number of incidents per year, but this could be caused by the reporting methodology. In the past, Barcelona

City Council gathered water related incidents through phone calls from citizens. Today, BCASA manages the database and has changed the way in which information is obtained. They want to obtain a greater variety of rain-related incidents, in order to create a more robust database. Table 2 shows the annual distribution of the rainfall episodes with reported incidents. In all the winter seasons, no episode was reported with these characteristics. The episodes with the highest alert level are most concentrated in autumn seasons. Nevertheless, the number of those events reported during summers is also significant. Overall, there is a similar number of cases with NAB = 3, spread over the spring, summer and autumn periods.

Table 2: Seasonal distribution of episodes with the most impact in Barcelona with reported incidents from April 2013 to December 2018. The seasons considered were winter (December, January, and February), spring (May, April, and March), summer (June, July, and August) and autumn (September, October, and November). The values shown are: the number of episodes for each category (NAB euqel to 3 or 4) per season, observed maximum, minimum and median values for maximum cumulated precipitation in an episode for each season, and 25 and 75 percentiles for the same variable for each season.

NAB	3						4					
	No. of Ep.	Max	Min	Med	25%	75%	No. of Ep.	Max	Min	Med	25%	75%
Winter	0	-	-	-	-	-	0	-	-	-	-	-
Spring	4	33.00	12.40	26.85	26.23	38.65	2	101.20	57.80	79.50	68.65	90.35
Summer	3	26.15	30.35	35.60	65.80	28.80	5	65.80	28.80	44.40	39.40	55.3
Autumn	5	40.30	37.50	53.30	133.40	28.10	9	133.40	28.10	94.90	45.50	101.2

After analysing the maximum cumulative precipitation (BCASA network) on the previously sub-selected episodes with reported incidents (Table 2), the ones with NAB equal to 3 indicate a maxima between 12.45 and 40.30 mm. Episodes with NAB equal to 4 showed a wider range of values: there are episodes with maximums from 28.10 to more than 110 mm (cumulative rainfall over 24 hours) and an exceptional case with 133.4 mm. Table 2 also displays seasonal variability of maximums collected in those rainfall episodes. Higher maximum values are observed in both spring and autumn seasons. Looking at the 75% percentile, episodes with NAB = 3 have larger rainfall accumulations in spring, while for those with NAB = 4, the larger accumulations occur during autumn.

When trying to establish trends and patterns in terms of impacts on the city of Barcelona, it seems that the number of episodes with reported incidents shows a decreasing trend over the years studied, except for 2018, where an unusual high number of extraordinary rainfall episodes compromised the normal running of the city. There is no doubt that rainwater management systems (such as rainwater tanks) and correct maintenance of the sewerage system, coordinated by BCASA, have had an important role on decreasing damage in the city [8], which again highlights the importance of early warning systems in order to be prepared against the most significant events.

3.2. Comparison of rain gauge data and radar data for rainfall episodes

For each episode on the database, maximum cumulative precipitation on rain gauge locations from radar products and rain gauge data are compared, as explained in the section 2.3.2 of methodology. For the 207 cases presented in the previous section, the overall difference (BIAS) is calculated, as well as the RMSE. In Figure 6, the seasonal distribution of the results in the comparison is shown. Episodes with no observational rain gauge data (3 of them) are counted as radar overestimation cases. For some months (from May to October) the radar struggled to reproduce the observations from the BCASA network, and

a trend to rainfall overestimation is observed. This is a consequence of using a single Z-R relationship throughout the year. Radar QPE calculations do not distinguish the water phase, but when there is ice in the clouds, the reflectivity values are much higher than usual and the resulting QPE may be much higher than the real figures. This applies for hail episodes (relatively frequent in Catalonia and the ROI [29]).

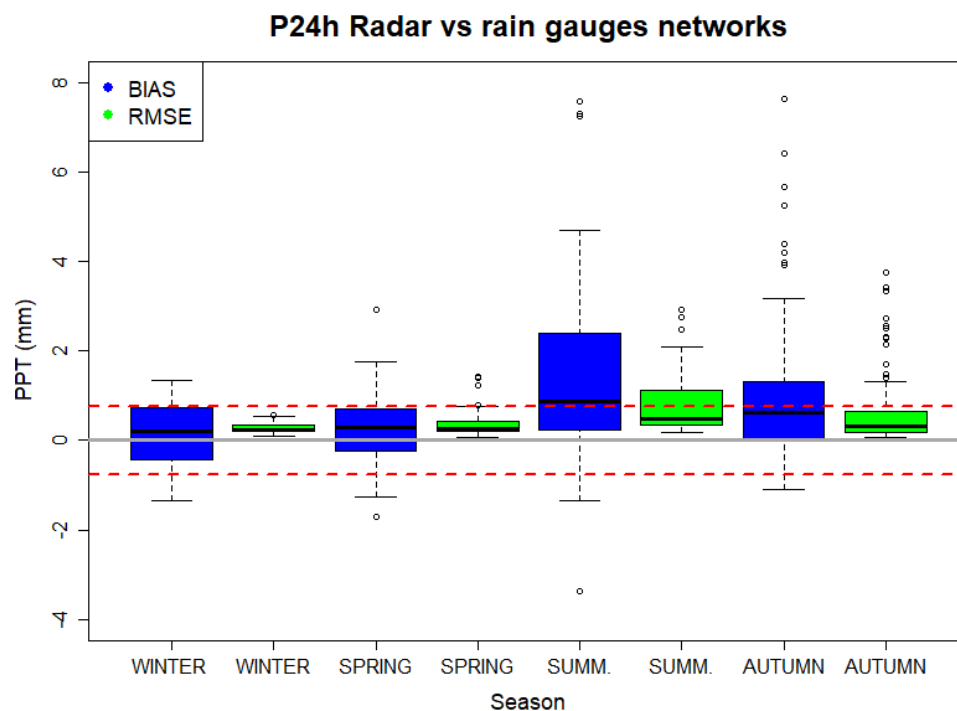


Figure 6: Seasonal distribution of the calculated 24h rainfall BIAS and RMSE between XRAD products and the BCASA rain gauge network for the 207 rainfall episodes in the ROI.

SMC had previously calculated the overall bias of its radar network in Catalonia. For each episode, they compared, point by point, the accumulated precipitation with the observations from an automatic weather station network (XEMA), also managed by the SMC. From June to September, SMC gets an overall positive bias, which is consistent with the results in Figure 6. But in this work, the positive bias also extends to October. This is also consistent with the SMC calculations, as they also documented a positive bias along the coastline of Catalonia from September to November. However, overall, this bias is compensated with a negative bias inland (not shown).

By comparing maximum cumulative precipitation values from both sources for episodes with NAB greater than or equal to 3, a trend towards radar overestimation can be observed. A larger study with a greater number of episodes with the same characteristics is needed to analyse this tendency in more detail. With the available data, it seems XRAD has a better ability to reproduce more accurate maximum values when NAB is equal to 3 than when it is equal to 4. It is also important to note that the rain gauge network is not as dense as the radar resolution data, so for highly convective precipitation with wide intensity gradients, radar measurements may be more accurate [25].

3.4. Storm hotspot analysis with radar

3.4.1. Analysis of surface maximum reflectivity maps

For significant episodes, the frequency of exceeding a surface reflectivity of 30 dBZ is shown (Figure 7). The procedure is repeated two more times, raising the target threshold to surpass a surface reflectivity of 45 dBZ (Figure 8) and once again for 55 dBZ (not shown).

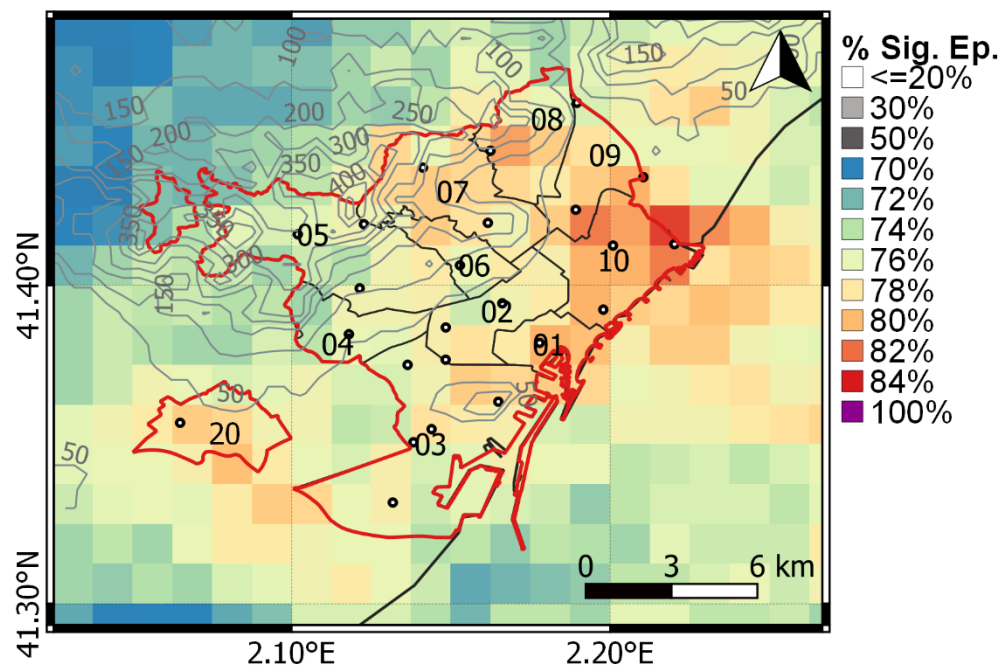


Figure 7: Distribution of maximum surface reflectivity surpassing 30 dBZ. It shows the frequency on each pixel for significant rainfall episodes. The grey contour lines show regions of a constant height (m). The red solid line outlines the ROI. Inside, black solid lines divide the different districts labelled as follows: 01 – Ciutat Vella, 02 – Eixample, 03 – Sants-Montjuïc, 04 – Les Corts, 05 – Sarrià, 06-Sant Gervasi, 07 – Horta-Guinardó, 08 - Nou Barris, 09 – Sant Andreu, 10 – Sant Martí, and 20 – Cornellà de Llobregat.

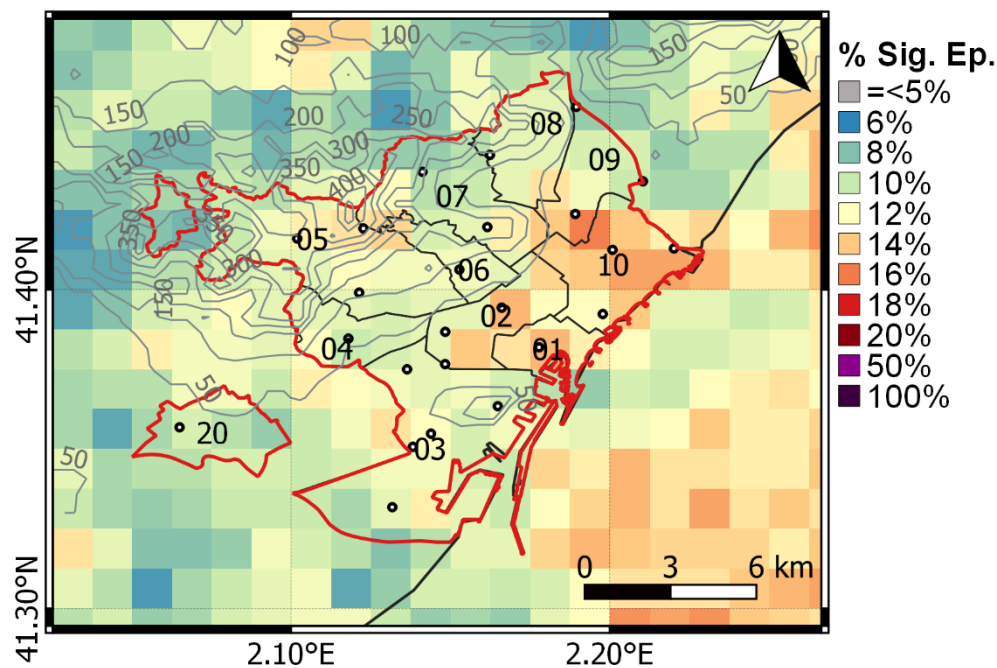


Figure 8: Same as Figure 7, for 45 dBZ.

Figure 7 shows a greater concentration of pixels with the highest frequencies in the north-eastern part of the ROI, mostly near the coast. In the Sant Martí district, for more than 81% of the cases, maximum surface reflectivity exceeds 30 dBZ. Another hotspot can be observed in Ciutat Vella and Nou Barris (for more than 80% of significant episodes). Also, Cornellà de Llobregat, Sant Andreu and Horta-Guinardó surpass the threshold in up to 80% of the studied episodes. When repeating the procedure with the 45 dBZ threshold, the number of significant episodes exceeding the threshold significantly decrease (Figure 8), but three different areas have a higher frequency of episodes surpassing the threshold. This occurs in the Sant Martí and Sant Andreu districts, with maximum frequencies up to 16%, in Ciutat Vella and Eixample with frequencies around 15%, and locally in the north-eastern part of Sarrià with 14% of cases. On the other hand, surface reflectivity values above 55 dBZ are rarely achieved inside the ROI, just in 1% of the significant episodes analysed for some of the pixels inside Sarrià and Ciutat Vella districts (not shown).

3.4.2. Analysis of convective cells on rainfall episodes

The algorithm was applied to the 207 rainfall episodes to identify convective cells within the area (ROI and a surrounding 10 km buffer). As a result, more than 8000 centroids of convective cells from 189 cases were obtained. **Error! Reference source not found.** shows the spatial distribution of these centroids inside ROI. A higher density of centroids was identified in four different zones:

- In the north-north-eastern part of the city, mostly affecting the Nou Barris and Horta-Guinardó districts, and the northern part of the Gràcia district.
- Right in the middle of the city, affecting the Eixample district, southern Gràcia and northern Sants-Montjuïc.
- The west part of the municipality of Cornellà de Llobregat.
- In the northwest of the Sant Martí district.

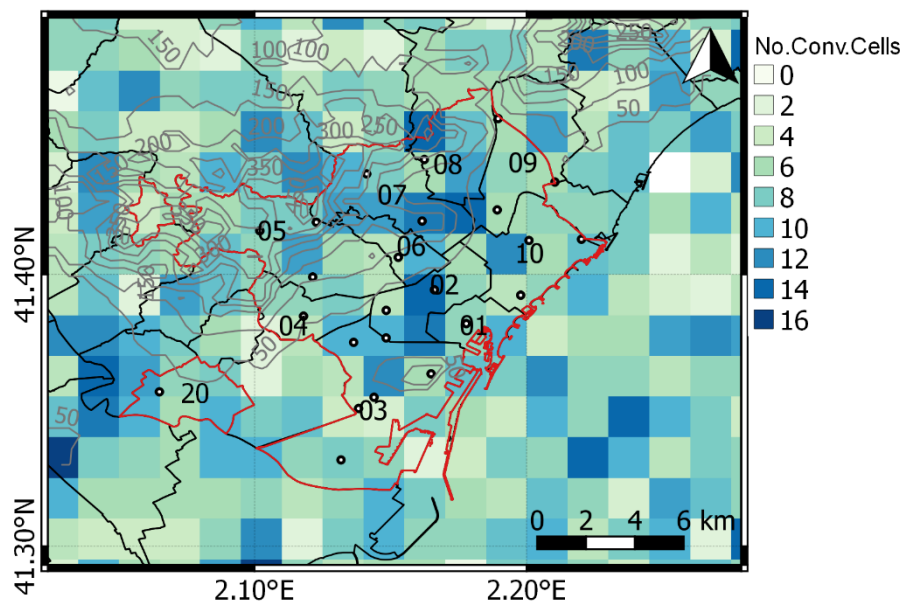


Figure 9: Distribution of centroids of convective cells for significant episodes. The numbers refer to Barcelona districts, and they are detailed on Figure 7.

Some of the mentioned districts also had high rates of surpassing the 45 dBZ threshold for surface reflectivity. Nevertheless, when comparing spatial distributions between Figure 8 and Figure 9, they are not so similar. While maximum surface reflectivity values over 45 dBZ are more prone to occur near the coast-line, the centroids of storm cells tend to concentrate more inland, right in the middle of the studied area.

For all the episodes with an NAB greater than or equal to 3, one or more convective cells were found by the algorithm. When analysing the hourly distribution of convective cells for these episodes, two maximums were obtained:

- Around 07:00 UTC time (in the morning), a relative maximum.
- From 15:00 to 20:00 UTC time (afternoon), reaching the peak at 17:00 UTC.

These results are consistent with a diurnal convection cycle, with the first maxima right after convection starts, due to diurnal heating, and the second one after the peak, causing convection to develop. Nonetheless, it is worth mentioning that a lower frequency of convective storm cells was expected during the night, especially during the early hours of the day. One possible explanation could be related with anomalous propagation on radar display. During steady nights where a temperature inversion was more likely, anomalous propagation may generate false echoes of intense reflectivity and the effect is most prone to occur in coastal regions [34,35]. Those echoes can be wrongly identified as storm cells.

Although the ensemble of episodes with greater NAB is limited, Figure 10 shows the spatial distribution of centroids (a) and the same for episodes with reported incidents.

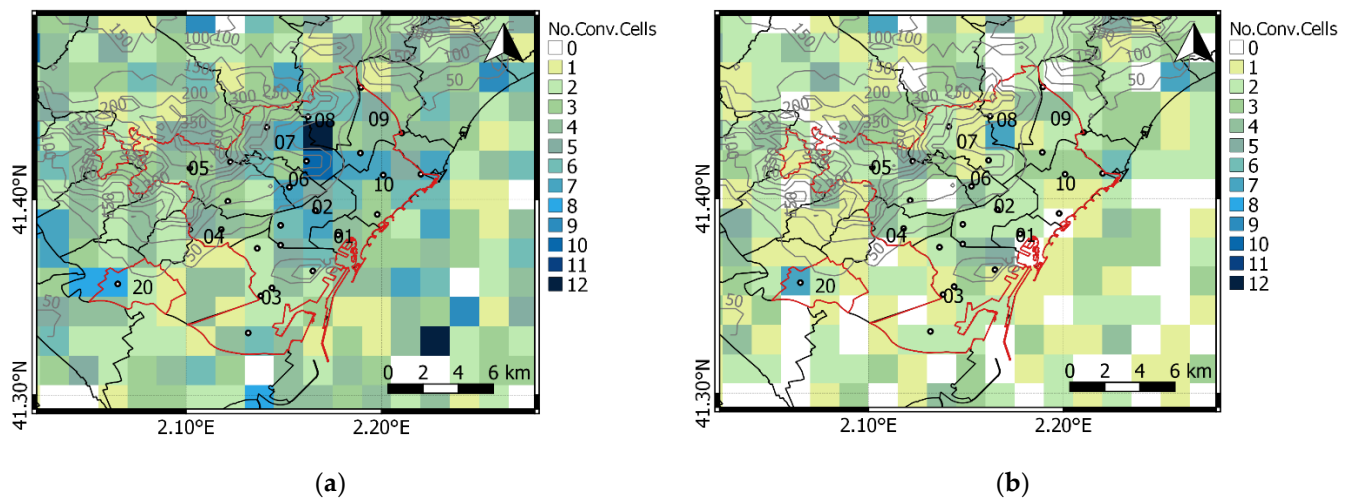


Figure 10: Distribution of storm cells centroids across all episodes with NAB 3 or 4 (a) and for episodes with the mentioned NAB levels and also, reported incidents (b).

When comparing Figure 9 and Figure 10, some common features are revealed. Pixels with the highest concentrations of centroids are located on the lower side of complex terrain, with a higher number of centroids per pixel in the middle of the ROI. Darker pixels on Figure 10 (a) are similar to those on Figure 9, but with a smaller number of centroids per pixel and a larger gradient between the most affected districts and the ones that are not so affected. Both figures agree that most of the centroids are found in the districts of Nou Barris, Horta-Guinardó, Eixample and Sants-Montjuïc. On the other side, Figure 10 (b) highlight maximum concentrations on Cornellà and on the border between Nou Barris and Horta-Guinardó districts. Also, some pixels have slightly higher concentration of centroids on the southern part of Gràcia, on Sarrià and les Corts and on the border between Montjuïc, Ciutat Vella and Eixample.

4. Conclusions

During this research, a new methodology was established to identify storm episodes in the city of Barcelona. A database was created by combining data from the BCASA rain gauge network and XRAD radar products from April 2013 to December 2018. The methods used were also able to identify some areas in the city with a greater concentration of storm centroids than others. The following paragraphs summarise the conclusions reached.

Identifying rainfall episodes with XRAD data results in a greater number of episodes than using data from the BCASA rain gauge network. The difference relays on limitations on the coverage for the rain gauge network, anomalous propagation of the radar beam under certain atmospheric conditions [34] or also to other anomalous echoes that may identify precipitating nuclei when they do not exist. During the winter, XRAD performed well in reproducing maximum cumulated precipitations in Barcelona. However, throughout May, June, August, September and October, there is a trend towards radar overestimation of the maximum cumulated rainfall.

Rainfall episodes with a greater impact on Barcelona are not the only factor linked to flood hazards, and vulnerability and exposure also play an important role [3]. That explains why on some intense rainfall episodes, few or no incidents were reported. Along the same lines, episodes with a significant impact on the city, but without large rainfall accumulations were also found. The year with the highest number of episodes with incidents was 2014. Even so, the greatest number of incidents per episode occurred in 2018.

BCASA rainwater management has contributed to reducing the number of episodes with reported incidents per year. However, during 2018 there was anomaly with a greater number of extremely intense rainfall episodes that compromised the normal running of the city.

Greater concentrations of convective cells centroids were identified on the lower side of the complex orography of Barcelona, with a greater incidence in some areas inside the districts of Cornellà de Llobregat, Nou Barris, Horta-Guinardó, Gràcia, Montjuïc, Ciutat Vella and Eixample. Also, locations more prone to surpass 45 dBZ were proven to be near the coastline, and do not exactly match the areas with the greatest concentration of storm centroids. This means that, even when the intensity of radar reflectivity is related to rainfall intensity, it is not the only factor to monitor to prevent flash floods. Some intense storms may not have high intensity values of reflectivity, but may still have a high impact.

Finally, for rainfall episodes with an NAB level of 3 or 4, a higher concentration of convective cells is found in the middle of the city. The time distribution of these cells shows the overlap of two phenomena: maximum number of convective cells agrees with the maxima for convection activity (diurnal heating) and the rate of convective cells with reported incidents its much higher from 6 UTC to 20 UTC, when the population is active. Also, the unexpectedly large number of centroids identified at night may be a result of anomalous propagation, unfiltered by the radar.

Although this study focused on a small area, a more detailed analysis would provide greater understanding of flash floods in Barcelona. A wider study period is needed and impacts on the city must be gathered more robustly. Also, the usage of urban meteorological and hydrological models should be considered. For all these reasons, the role of specific institutions, such as BCASA, is increasingly important. Data needs to be stored, cleaned, and analysed in robust ways, and monitoring and management systems need to be continually reviewed and improved in order to increase resilience to flash floods in Barcelona.

Author Contributions: Conceptualisation, L.E., M.L. and T. R.; methodology, L.E. and T.R.; software, L.E.; validation, L.E. T.R., B.A. and M.L.; writing—original draft preparation, L.E.; writing—review and editing, M.L. and T.R. All authors have read and agreed to the published version of the manuscript.

Funding: This research received no external funding.

Institutional Review Board Statement: Not applicable.

Informed Consent Statement: Not applicable.

Data Availability Statement: Not applicable.

Acknowledgments: This work was carried out under the framework of the SINOPTICA (H2020-SESAR-2019-2, 892362) European project of Horizon 2020 and the M-CostAdapt (CTM2017-83655-C2-2-R) research project, funded by the Spanish Ministry of Economy and Competitiveness (MINECO/AEI/FEDER, UE). The authors would like to thank to BCASA for their commitment, collaboration, and data. Thanks also go to the Meteorological Service of Catalonia for their collaboration and the data provided. Finally, thanks go to the Water Research Institute (Instituto de Investigación del Agua - IdRA) and the SINOPTICA (H2020-SESAR-2019-2, 892362) European project of Horizon 2020 for enabling this paper to be written. Thank you to Hannah Bestow for her revision of the English.

Conflicts of Interest: The authors declare no conflict of interest.

Appendix A

Table A.1: List of the 207 rainfall episodes inside ROI resulting from the combination of XRAD and BCASA data

Date	P _{max} BCASA	P _{max} XRAD	Date	P _{max} BCASA	P _{max} XRAD	Date	P _{max} BCASA	P _{max} XRAD	Date	P _{max} BCASA	P _{max} XRAD
25/04/2013	17.4	16.2	17/09/2014	4.3	13.0	22/07/2016	18.6	21.9	26/01/2018	62.1	51.5
27/04/2013	23.6	28	22/09/2014	9.7	20.1	30/08/2016	12.3	13.0	01/02/2018	16.2	10.0
28/04/2013	13.4	14.4	23/09/2014	6.0	10.0	10/09/2016	11.5	5.0	04/02/2018	27.9	38.9
29/04/2013	16.7	27.8	28/09/2014	95.4	101.2	13/09/2016	24.9	28.1	05/02/2018	39.2	39.9
15/05/2013	32.7	38.3	29/09/2014	21.3	7.0	14/09/2016	18.2	20.8	08/02/2018	45.2	16.8
16/05/2013	6.7	17.7	30/09/2014	46.3	35.3	23/09/2016	57.4	69.4	12/02/2018	20.6	19.0
18/05/2013	7.9	10.8	05/10/2014	12.4	17.8	06/10/2016	31.5	28.1	28/02/2018	13.9	15.9
19/05/2013	16.5	23.8	03/11/2014	44.6	45.5	12/10/2016	61.1	77.7	20/03/2018	45.4	35.4
20/05/2013	10.3	12.1	04/11/2014	18.9	15.3	13/10/2016	62.2	54.0	24/03/2018	58.4	47.7
08/06/2013	25.1	28.8	26/11/2014	35.4	35.3	22/10/2016	8.2	10.0	26/03/2018	13.5	16.0
21/06/2013	5.6	15.5	27/11/2014	14.4	16.4	22/11/2016	12.6	13.4	08/04/2018	10.3	9.0
18/07/2013	33.4	36	29/11/2014	52.1	40.3	23/11/2016	28.5	32.5	10/04/2018	10.0	8.0
29/07/2013	3.8	12.1	30/11/2014	40.4	53.3	27/11/2016	14.0	21.9	11/04/2018	35.4	30.7
26/08/2013	19.3	15.5	15/12/2014	18.6	18.0	16/12/2016	19.3	16.5	13/04/2018	6.3	10.7
27/08/2013	2	19.4	19/01/2015	13.4	13.9	19/12/2016	16.9	17.9	14/04/2018	10.1	12.0
28/08/2013	2.6	15.1	04/02/2015	19.3	20.1	22/01/2017	6.9	13.0	01/05/2018	82.0	62.4
07/09/2013	24.4	23.2	05/02/2015	0.0	23.9	27/01/2017	23.6	23.1	13/05/2018	7.9	12.7
10/09/2013	1.5	83.4	04/03/2015	13.1	12.2	08/02/2017	14.2	16.4	22/05/2018	0.7	17.1
11/09/2013	18.2	10.2	14/03/2015	22.5	12.5	13/02/2017	19.1	15.8	29/05/2018	11.0	9.0
04/10/2013	14.1	15.8	21/03/2015	36.3	21.6	24/02/2017	15.7	14.7	03/06/2018	21.0	29.2
06/10/2013	10.4	24.7	26/03/2015	11.8	17.5	03/03/2017	16.2	13.0	06/06/2018	39.8	37.2
07/10/2013	17.2	55.8	19/05/2015	43.4	55.6	04/03/2017	12.7	10.0	07/06/2018	18.3	30.9
08/10/2013	0.6	13.1	20/05/2015	34.3	28.5	24/03/2017	107.4	101.2	28/06/2018	3.5	12.2
09/10/2013	3.8	14.1	11/06/2015	11.9	13.7	25/03/2017	24.1	25.6	16/07/2018	50.5	44.4
11/10/2013	13.4	11.2	15/06/2015	29.9	26.6	01/04/2017	15.4	13.1	22/07/2018	18.7	15.5
16/11/2013	40.1	56.7	16/06/2015	3.4	10.9	05/04/2017	9.1	10.1	17/08/2018	64.9	65.8
17/11/2013	43.4	62.9	31/07/2015	10.0	14.2	26/04/2017	12.9	10.6	25/08/2018	4.0	13.0
18/11/2013	41.4	49.3	01/08/2015	23.4	14.0	27/04/2017	25.4	22.9	30/08/2018	11.7	12.5
19/12/2013	10.1	11.5	13/08/2015	32.7	32.3	11/05/2017	21.9	16.8	31/08/2018	73.2	77.5
19/01/2014	35.4	25.1	15/08/2015	17.0	17.5	04/06/2017	24.0	24.1	01/09/2018	14.2	15.7
29/01/2014	28.8	26.7	18/08/2015	18.2	26.7	05/06/2017	10.3	12.2	06/09/2018	92.2	94.9
09/02/2014	13.9	13.6	10/09/2015	35.2	37.5	30/06/2017	8.9	12.9	07/09/2018	39.6	76.3
30/03/2014	13.2	14.3	23/09/2015	19.0	13.9	25/07/2017	25.3	46.7	12/09/2018	40.5	41.1
31/03/2014	10.9	12.2	29/09/2015	17.4	20.7	08/08/2017	14.0	14.2	15/09/2018	1.1	40.2
03/04/2014	55.9	57.8	30/09/2015	26.5	23.2	31/08/2017	19.6	18.5	18/09/2018	40.0	27.0
22/04/2014	30.5	12.4	03/10/2015	38.0	80.1	06/09/2017	11.1	20.8	07/10/2018	21.2	26.3
26/05/2014	26.0	33.0	07/10/2015	38.9	69.4	09/09/2017	21.3	30.7	09/10/2018	102.8	118.2
28/05/2014	28.1	25.2	08/10/2015	5.6	17.9	12/09/2017	7.5	33.2	10/10/2018	21.9	21.7
30/05/2014	17.7	19.4	13/10/2015	13.9	22.2	14/09/2017	14.7	14.2	13/10/2018	14.0	12.2
15/06/2014	27.7	38.9	26/10/2015	9.0	17.0	15/09/2017	8.0	10.0	14/10/2018	44.5	49.8
16/06/2014	7.0	14.4	27/10/2015	7.8	14.9	18/09/2017	6.1	13.6	19/10/2018	18.9	28.9
17/06/2014	14.3	28.4	02/11/2015	60.6	52.8	22/09/2017	37.1	17.8	27/10/2018	29.9	31.2
04/07/2014	17.0	17.8	03/11/2015	7.2	53.4	26/09/2017	9.4	19.0	28/10/2018	9.8	14.1
07/07/2014	30.0	47.2	27/02/2016	30.4	26.4	01/10/2017	13.4	35.8	29/10/2018	0.0	12.6

28/07/2014	30.5	39.4	16/03/2016	29.4	19.7	18/10/2017	29.4	27.8	31/10/2018	60.1	52.5
29/07/2014	6.6	15.1	20/03/2016	23.8	18.4	19/10/2017	92.0	95.4	05/11/2018	9.9	11.9
02/08/2014	11.9	16.9	01/04/2016	19.5	19.2	20/10/2017	6.1	14.2	09/11/2018	37.7	32.1
15/08/2014	14.4	19.9	05/04/2016	21.5	21.3	04/11/2017	10.8	14.6	14/11/2018	2.6	11.0
22/08/2014	54.3	55.3	21/04/2016	30.0	35.3	25/11/2017	9.0	16.3	15/11/2018	138.5	133.4
05/09/2014	10.9	14.1	18/06/2016	28.8	23.9	02/12/2017	0.0	21.4	18/11/2018	18.7	12.1
14/09/2014	18.8	27.3	13/07/2016	4.8	12.8	07/01/2018	13.9	19.5	20/11/2018	11.0	10.9
16/09/2014	20.3	46.8	14/07/2016	0.9	24.0	13/01/2018	9.3	11.2			

Table A.2: Rainfall episodes in Barcelona with NAB levels greater than or equal to 3. Maximum cumulative values of precipitation from radar data and rain gauges data are also provided along with the NAB level achieved and the number of incidents reported to Barcelona City Council.

Date	P _{max} Rad	P _{max} BCASA	NAB	Incidents
08/06/2013	28.8	25.1	4	15
18/07/2013	36.0	33.4	4	
07/09/2013	23.2	24.4	3	
04/10/2013	15.8	14.1	3	
17/11/2013	62.9	43.4	3	
19/01/2014	25.1	35.4	4	
29/01/2014	26.7	28.8	3	
03/04/2014	57.8	55.9	4	29
22/04/2014	12.4	30.5	3	
26/05/2014	33.0	26.0	3	28
28/05/2014	25.2	28.1	3	
30/05/2014	19.4	17.7	3	8
15/06/2014	38.9	27.7	3	6
17/06/2014	28.4	14.3	3	2
04/07/2014	17.8	17.0	3	
07/07/2014	47.2	30.0	3	
28/07/2014	39.4	30.5	4	20
29/07/2014	15.1	6.6	3	
02/08/2014	16.9	11.9	3	
15/08/2014	19.9	14.4	3	
22/08/2014	55.3	54.3	4	8
14/09/2014	27.3	18.8	3	
16/09/2014	46.8	20.3	3	
28/09/2014	101.2	95.4	4	26
30/09/2014	35.3	46.3	3	
03/11/2014	45.5	44.6	4	34
26/11/2014	35.3	35.4	3	7
29/11/2014	40.3	52.1	3	5
30/11/2014	53.3	40.4	3	1
19/05/2015	55.6	43.4	3	1
20/05/2015	28.5	34.3	3	4
01/08/2015	14.0	23.4	3	
13/08/2015	32.3	32.7	3	4
15/08/2015	17.5	17.0	3	
10/09/2015	37.5	35.2	3	6
29/09/2015	20.7	17.4	3	

30/09/2015	23.2	26.5	3	
03/10/2015	80.1	38	3	1
07/10/2015	69.4	38.9	3	
02/11/2015	52.8	60.6	4	2
20/03/2016	18.4	23.8	3	
18/06/2016	23.9	28.8	3	
13/09/2016	28.1	24.9	3	
23/09/2016	69.4	57.4	3	
06/10/2016	28.1	31.5	4	58
13/10/2016	54.0	62.2	3	
24/03/2017	101.2	107.4	4	11
25/07/2017	46.7	25.3	3	
31/08/2017	18.5	19.6	3	
19/10/2017	95.4	92.0	4	64
26/01/2018	51.5	62.1	3	
01/05/2018	62.4	82.0	3	
06/06/2018	37.2	39.8	3	
16/07/2018	44.4	50.5	4	72
17/08/2018	65.8	64.9	4	25
31/08/2018	77.5	73.2	3	
06/09/2018	94.9	92.2	4	72
07/09/2018	76.3	39.6	3	
12/09/2018	41.1	40.5	4	11
18/09/2018	27.0	40.0	3	
09/10/2018	118.2	102.8	4	79
14/10/2018	49.8	44.5	3	
09/11/2018	32.1	37.7	3	
15/11/2018	133.4	138.5	4	94

References

1. Marchi, L.; Borga, M.; Preciso, E.; Gaume, E. Characterisation of Selected Extreme Flash Floods in Europe and Implications for Flood Risk Management. *J. Hydrol.* **2010**, *394* (1–2), 118–133. <https://doi.org/10.1016/j.jhydrol.2010.07.017>.
2. Llasat, M. C.; Barriendos, M.; Barrera, A.; Rigo, T. Floods in Catalonia (NE Spain) since the 14th Century. Climatological and Meteorological Aspects from Historical Documentary Sources and Old Instrumental Records. *J. Hydrol.* **2005**, *313* (1–3), 408–418. <https://doi.org/10.1016/j.jhydrol.2005.02.004>.
3. Llasat, M. C.; Llasat-Botija, M.; Rodriguez, A.; Lindbergh, S. Flash Floods in Catalonia: A Recurrent Situation. *Adv. Geosci.* **2010**, *26*, 105–111. <https://doi.org/10.5194/adgeo-26-105-2010>.
4. Barnolas, M.; Llasat, M. C. A Flood Geodatabase and Its Climatological Applications: The Case of Catalonia for the Last Century. *Natural Hazards and Earth System Science*. European Geosciences Union 2007, pp 271–281. <https://doi.org/10.5194/nhess-7-271-2007>.
5. Cortès, M.; Llasat, M. C.; Gilabert, J.; Llasat-Botija, M.; Turco, M.; Marcos, R.; Martín Vide, J. P.; Falcón, L. Towards a Better Understanding of the Evolution of the Flood Risk in Mediterranean Urban Areas: The Case of Barcelona. *Nat. Hazards* **2018**, *93* (1), 39–60. <https://doi.org/10.1007/s11069-017-3014-0>.
6. Gascón, E.; Laviola, S.; Merino, A.; Miglietta, M. M. Analysis of a Localized Flash-Flood Event over the Central Mediterranean. *Atmos. Res.* **2016**, *182*, 256–268. <https://doi.org/10.1016/j.atmosres.2016.08.007>.

7. Llasat, M. C.; Marcos, R.; Turco, M.; Gilabert, J.; Llasat-Botija, M. Trends in Flash Flood Events versus Convective Precipitation in the Mediterranean Region: The Case of Catalonia. *J. Hydrol.* **2016**, *541*, 24–37. <https://doi.org/10.1016/j.jhydrol.2016.05.040>.
8. Barrera, A.; Llasat, M. C.; Barriendos, M. Estimation of Extreme Flash Flood Evolution in Barcelona County from 1351 to 2005. *Nat. Hazards Earth Syst. Sci.* **2006**, *6* (4), 505–518. <https://doi.org/10.5194/nhess-6-505-2006>.
9. Llasat, M. C.; Marcos, R.; Llasat-Botija, M.; Gilabert, J.; Turco, M.; Quintana-Seguí, P. Flash Flood Evolution in North-Western Mediterranean. *Atmos. Res.* **2014**, *149*, 230–243. <https://doi.org/10.1016/j.atmosres.2014.05.024>.
10. Llasat, M. C.; López, L.; Barnolas, M. Flash-Floods in Catalonia: The Social Perception in a Context of Changing Vulnerability. *Adv. Geosci.* **2008**, *17*, 63–70. <https://doi.org/10.5194/adgeo-17-63-2008>.
11. Blöschl, G.; Viglione, A.; Montanari, A. Emerging Approaches to Hydrological Risk Management in a Changing World. *Climate Vulnerability: Understanding and Addressing Threats to Essential Resources*. Elsevier Inc. 2013, pp 3–10. <https://doi.org/10.1016/B978-0-12-384703-4.00505-0>.
12. Llasat, M. C.; Llasat-Botija, M.; López, L. A Press Database on Natural Risks and Its Application in the Study of Floods in Northeastern Spain. *Nat. Hazards Earth Syst. Sci.* **2009**, *9* (6), 2049–2061. <https://doi.org/10.5194/nhess-9-2049-2009>.
13. Nakamura, I.; Llasat, M. C. Policy and Systems of Flood Risk Management: A Comparative Study between Japan and Spain. *Nat. Hazards* **2017**, *87* (2), 919–943. <https://doi.org/10.1007/s11069-017-2802-x>.
14. United Nations for Disaster Risk Reduction. *Hazard Definition & Classification Review*; 2020.
15. Pachauri, R. K.; Meyer, L.; Allen, M. R.; Barros, V. R.; Broome, J.; Cramer, W.; Jiang, K.; Jiménez Cisneros México, B.; Kattsov, V.; Lee, H.; Minx, J.; Mulugetta, Y.; Brinkman, S.; van Kesteren, L.; Leprince-Ringuet, N.; van Boxmeer, F. *IPCC, 2014: Climate Change 2014: Impacts, Adaptation, and Vulnerability*; 2014.
16. Drost, R.; Casteel, M.; Libarkin, J.; Thomas, S.; Meister, M. Severe Weather Warning Communication: Factors Impacting Audience Attention and Retention of Information during Tornado Warnings. *Weather. Clim. Soc.* **2016**, *8* (4), 361–372. <https://doi.org/10.1175/WCAS-D-15-0035.1>.
17. Cortès, M.; Turco, M.; Llasat-Botija, M.; Llasat, M. C. The Relationship between Precipitation and Insurance Data for Floods in a Mediterranean Region (Northeast Spain). *Nat. Hazards Earth Syst. Sci.* **2018**, *18* (3), 857–868. <https://doi.org/10.5194/nhess-18-857-2018>.
18. Naylor, J.; Sexton, A. The Relationship between Severe Weather Warnings, Storm Reports, and Storm Cell Frequency in and around Several Large Metropolitan Areas. *Weather Forecast.* **2018**, *33* (5), 1339–1358. <https://doi.org/10.1175/waf-d-18-0019.1>.
19. Doswell III, C.; Ramis, C.; Romero, R.; Alonso, S. A Diagnostic Study of Three Heavy Precipitation Episodes in the Western Mediterranean Region. *Weather Forecast.* **1998**, *13* (1), 102–124. [https://doi.org/https://doi.org/10.1175/1520-0434\(1998\)013<0102:ADSOTH>2.0.CO;2](https://doi.org/https://doi.org/10.1175/1520-0434(1998)013<0102:ADSOTH>2.0.CO;2).
20. Rigo, T.; Llasat, M. C. A Methodology for the Classification of Convective Structures Using Meteorological Radar: Application to Heavy Rainfall Events on the Mediterranean Coast of the Iberian Peninsula. *Nat. Hazards Earth Syst. Sci.* **2004**, *4* (1), 59–68. <https://doi.org/10.5194/nhess-4-59-2004>.
21. Bech, J.; Vilaclara, E.; Pineda, N.; Rigo, T.; López, J.; O'hora, F.; Lorente, J.; Sempere, D.; Fàbregas, F. X. The Weather Radar Network of the Catalan Meteorological Service: Description and Applications. In *Proceedings of ERAD (2004)*; 2004; pp 416–420.
22. Cáceres, R.; Codina, B. Radar Data Assimilation Impact over Nowcasting a Mesoscale Convective System in

- Catalonia Using the WRF Model. *Tethys* **2018**, No. 15, 3–17. <https://doi.org/10.3369/tethys.2018.15.01>.
23. Rigo, T.; Berenguer, M.; Llasat, M. C. An Improved Analysis of Mesoscale Convective Systems in the Western Mediterranean Using Weather Radar. *Atmos. Res.* **2019**, 227 (May), 147–156. <https://doi.org/10.1016/j.atmosres.2019.05.001>.
 24. Trapero, L.; Bech, J.; Rigo, T.; Pineda, N.; Forcadell, D. Uncertainty of Precipitation Estimates in Convective Events by the Meteorological Service of Catalonia Radar Network. *Atmos. Res.* **2009**, 93 (1–3), 408–418. <https://doi.org/10.1016/j.atmosres.2009.01.021>.
 25. Steiner, M.; Smith, J. A.; Burges, S. J.; Alonso, C. V.; Darden, R. W. Effect of Bias Adjustment and Rain Gauge Data Quality Control on Radar Rainfall Estimation. *Water Resour. Res.* **1999**, 35 (8), 2487–2503. <https://doi.org/10.1029/1999WR900142>.
 26. Barcelona Cicle de l'Aigua, S. A.; CLABSA. Informe de pluja [versió resumida] : període del 21 de setembre al 22 de setembre de 1995 <https://bcnroc.ajuntament.barcelona.cat/jspui/handle/11703/118351> (accessed Mar 1, 2021).
 27. Pere Malgrat Bregolat, Albert Vilalta i Cambra, J. M. V. Los depositos de retencion de aguas pluviales de Barcelona: un nuevo enfoque en la lucha contra las inundaciones y la proteccion medioambiental <https://www.osti.gov/etdeweb/biblio/20567346> (accessed Apr 7, 2021).
 28. Gjertsen, U.; Sálek, M. ˇ; Michelson, D. B. Gauge Adjustment of Radar-Based Precipitation Estimates in Europe. In *Proceedings of the ERAD (2004)*; 2004; pp 7–11.
 29. Rigo, T.; Carmen Llasat, M. Forecasting Hailfall Using Parameters for Convective Cells Identified by Radar. *Atmos. Res.* **2016**, 169, 366–376. <https://doi.org/10.1016/j.atmosres.2015.10.021>.
 30. del Moral, A.; Rigo, T.; Llasat, M. C. A Radar-Based Centroid Tracking Algorithm for Severe Weather Surveillance: Identifying Split/Merge Processes in Convective Systems. *Atmos. Res.* **2018**, 213 (May), 110–120. <https://doi.org/10.1016/j.atmosres.2018.05.030>.
 31. Barnolas, M.; Rigo, T.; Llasat, M. C. Characteristics of 2-D Convective Structures in Catalonia (NE Spain): An Analysis Using Radar Data and GIS. *Hydrol. Earth Syst. Sci* **2010**, 14, 129–139. <https://doi.org/10.5194/hess-14-129-2010>.
 32. Peleg, N.; Morin, E. Convective Rain Cells: Radar-Derived Spatiotemporal Characteristics and Synoptic Patterns over the Eastern Mediterranean. *J. Geophys. Res. Atmos.* **2012**, 117 (15). <https://doi.org/10.1029/2011JD017353>.
 33. Llasat, M. C. An Objective Classification of Rainfall Events on the Basis of Their Convective Features: Application to Rainfall Intensity in the Northeast of Spain. *Int. J. Climatol.* **2001**, 21 (11), 1385–1400. <https://doi.org/10.1002/joc.692>.
 34. Bech, J.; Codina, B.; Lorente, J. Forecasting Weather Radar Propagation Conditions. *Meteorol. Atmos. Phys.* **2007**, 96 (3–4), 229–243. <https://doi.org/10.1007/s00703-006-0211-x>.
 35. Steiner, M.; Smith, J. A. Use of Three-Dimensional Reflectivity Structure for Automated Detection and Removal of Nonprecipitating Echoes in Radar Data. *J. Atmos. Ocean. Technol.* **2002**, 19 (5), 673–686. [https://doi.org/10.1175/1520-0426\(2002\)019<0673:UOTDRS>2.0.CO;2](https://doi.org/10.1175/1520-0426(2002)019<0673:UOTDRS>2.0.CO;2).